doi: 10.17221/8/2017-VETMED

Primary brain involvement of disseminated histiocytic sarcoma in a Rottweiler dog – histopathology, ^{18}F-fluorodeoxyglucose positron emission tomography and 7 T-magnetic resonance imaging findings: a case report

B.T. Kang[1*†], D. An[1], H.W. Kim[2], Y. Jin[3], Y.D. Son[4], D.I. Jung[5], J.H. Kang[1], M.P. Yang[1], J.H. Sur[2], S.R. Lee[3†]

[1]Veterinary Teaching Hospital, Chungbuk National University, Cheongju, Republic of Korea
[2]Small Animal Tumor Diagnostic Center, Konkuk University, Seoul, Republic of Korea
[3]The National Primate Research Center, Korea Research Institute of Bioscience and Biotechnology, Ochang, Republic of Korea
[4]College of Health Science, Gachon University, Incheon, Republic of Korea
[5]Institute of Animal Medicine, Gyeongsang National University, Jinju, Republic of Korea

*Corresponding author: kangbt@chungbuk.ac.kr

†These authors contributed equally to this work

ABSTRACT: An eight-year-old, intact male Rottweiler dog was presented due to anorexia, lethargy, ataxia and imbalance. Cerebellar and thyroid masses were identified using 0.3T magnetic resonance imaging. The ^{18}F-fluorodeoxyglucose uptakes of the masses were elevated on positron emission tomography and 7 T-magnetic resonance imaging fusion imaging. At 113 days after the initial presentation, new nodular lesions were observed in the skin, liver and spleen. Histopathology revealed multiple lesions of disseminated histiocytic sarcoma in the cerebellum, liver, spleen and skin, whereas the thyroid lesions were diagnosed as mixed medullary-follicular thyroid carcinoma. The primary site of the disseminated histiocytic sarcoma was found to be in the cerebellum. To our knowledge, this is the first case report to describe the imaging and histopathological findings of extracranial metastasis of a primary intracranial histiocytic sarcoma in a dog.

Keywords: mixed medullary-follicular thyroid carcinoma; canine; magnetic resonance imaging; positron emission tomography

Neoplastic histiocytic diseases in dogs encompass cutaneous histiocytoma and histiocytic sarcoma (localised, disseminated and haemophagocytic forms; Moore 2014). Histiocytic sarcoma (HS) is a malignant neoplasm mostly originating from interstitial dendritic cells, which can be localised to the bone, joints, skin and the subcutis, and can eventually be disseminated to the spleen, liver, lymph nodes, lungs, bone marrow and central nervous system (Affolter and Moore 2002; Moore 2014). Although disseminated HS is characterised by multiple neoplasms in several organs, the brain is not

Supported by the Basic Science Research Program through the National Research Foundation of Korea (NRF) funded by the Ministry of Education, Republic of Korea (Grant No. 2017R1D1A3B03028863).

doi: 10.17221/8/2017-VETMED

considered to be one of the primary sites for disseminated HS (Thio et al. 2006; Snyder et al. 2008).

Thyroid carcinomas represent 90% of thyroid tumours in dogs and can arise either from follicular cells (follicular thyroid carcinoma) or parafollicular cells (parafollicular, C cell or medullary thyroid carcinoma) (Kiupel et al. 2008; Wucherer and Wilke 2010). In addition to this classification of thyroid carcinomas, rare cases of medullary carcinoma accompanied by follicular-derived components have been described in humans (Hales et al. 1982; Pfaltz et al. 1983). Because these atypical tumours display morphological and immunoreactive features of both follicular and medullary thyroid carcinomas, they have been termed mixed medullary-follicular thyroid carcinomas (MMFC; Pfaltz et al. 1983; Sadow and Hunt 2010).

The aim of this case report was to describe the clinical, imaging and histopathologic findings of disseminated HS with primary brain involvement and concurrent MMFC in a dog. To the authors' knowledge, this is the first report of disseminated HS in which cerebellar dendritic cells likely represented the primary site of neoplasia.

Case description

An eight-year-old, intact male Rottweiler dog presented with a three-week history of anorexia, lethargy, ataxia and difficulty in maintaining balance. Two firm and fixed subcutaneous masses (length × thickness: 120 mm × 45 mm on the left, 101 mm × 29 mm on the right) were palpated on the ventral neck bilaterally. On neurological examination, the dog appeared mentally depressed with non-ambulatory tetraparesis, titubation and intention tremors. The thoracic limbs were slightly hypertonic, whereas all cranial nerves and spinal reflexes were normal, suggesting a brain lesion localised to the cerebellum and brain stem.

A complete blood count showed mild lymphopaenia (720/µl; reference range 1000–4800/µl). Elevated levels of alanine aminotransferase (2.53 µkat/l; reference range 0.36–1.73 µkat/l), alkaline phosphatase (52.04 µkat/l; reference range 0.49–1.65 µkat/l) and blood urea nitrogen (13.14 mmol/l; reference range 2.50–8.92 mmol/l) were observed on the serum chemistry panel. Thoracic radiographs revealed multiple small nodules with soft tissue opacities in the whole lung lobes, including a large solitary nodule (32 mm × 50 mm) in the left cranial lobe. Moderate vascularisation, intact tumour capsule, enlargement (length × diameter: 98 mm × 29 mm on the left, 83 mm × 19 mm on the right), and heterogeneous parenchymal echogenicity of both sides of the thyroid glands were observed on ultrasonography. Ultrasound-guided fine-needle aspiration of the thyroid gland revealed densely clustered cells with rather uniform nuclei and pale cytoplasm. Computed tomography (CT) scan of the whole body was performed with a peak voltage of 120 kV, amperage of 130 mA, and slice thickness of 7 mm. Images were obtained before and after intravenous administration of iohexol (Omnipaque, GE Healthcare, Buckinghamshire, UK) at 525 mg/kg body weight. CT demonstrated round masses on both sides of the thyroid gland (length × diameter: 112 mm × 39 mm on the left, 94 mm × 25 mm on the right). Moderate enhancement (difference in attenuation of 50 to 100 Hounsfield units) was noted in both masses after injection of contrast agent. On thyroid function tests, slightly decreased values of serum T4 (total T4, 6.05 nmol/l [reference range 12.87–51.49 nmol/l]; free T4, 7.08 pmol/l [reference range, 7.72–47.62 pmol/l]) and a normal serum level of endogenous thyrotropin (thyroid-stimulating hormone, 0.23 ng/ml; reference range 0.05–0.42 ng/ml) were found. No abnormalities were noted on abdominal radiography, ultrasonography or CT.

Because a cerebellar lesion was suspected, magnetic resonance imaging (MRI) of the brain was performed using a 0.3T MR scanner (AIRIS II, Hitachi Medical Corp, Tokyo, Japan). T2-weighted images (WI; TR 3456 ms, TE 90 ms, flip angle 90°, matrix 256 × 256, field of view (FOV) 170 mm × 170 mm, slice thickness 5 mm, interslice gap 5.5 mm) and pre-contrast (TR 315 ms, TE 14 ms, flip angle 90°, matrix 256 × 256, FOV 170 mm × 170 mm, slice thickness 5 mm, interslice gap 5.5 mm) and post-contrast T1-WI (TR 393 ms, TE 14 ms, flip angle 90°, matrix 256 × 256, FOV 170 mm × 170 mm, slice thickness 3 mm, interslice gap 3.5 mm) were acquired in the transverse, sagittal and dorsal planes. A cerebellar mass was identified as a circular, isointense to hypointense structure on T1-WI, with a mixed signal intensity on T2-WI. The fourth ventricle and medulla oblongata were compressed by the mass. After intravenous administration of gadolinium-diethylenetriamine pentaacetic acid (Magnevist, Bayer Healthcare, Whippany, USA),

doi: 10.17221/8/2017-VETMED

signal intensity was increased in the cerebellar mass. The diameter of the mass and of the enhanced area was 15–17 mm. Additional T2-WI of the thyroid glands demonstrated hyperintensities with heterogeneous parenchymal texture. Mononuclear pleocytosis (12 cells/µl; reference range 0–5 cells/µl) and increased protein concentration (0.89 g/l; reference range 0–0.25 g/l) were found on cerebrospinal fluid analysis.

Because primary brain tumours rarely metastasise outside the brain, a thyroid tumour with intracranial and pulmonary metastases was strongly suspected, and incisional biopsies of the thyroid glands was recommended. However, the owner refused this invasive procedure and requested an initiation of chemotherapy. Based on the presumptive diagnosis of a malignant thyroid tumour, the dog was initially treated with carboplatin (300 mg/m^2 *i.v.* once every 2–3 weeks; Carbotinol, Korea United Pharm., Sejong, Republic of Korea) and prednisolone (1 mg/kg *s.c. q* 12 h; Solondo, Yuhan Corp., Ochang, Republic of Korea). The dog became alert and the thoracic limb rigidity, tetraparesis, involuntary movements, neck masses and pulmonary nodules were all alleviated after the second cycle of chemotherapy.

Six weeks after the initial presentation, cerebellar and cervical lesions were monitored by positron emission tomography (PET) and 7 T MRI fusion imaging, with the owner's permission. The dog was fasted for 12 h, and then injected intravenously with ^{18}F-fluorodeoxyglucose (FDG; 14.8 MBq). The dog was kept caged for one hour to ensure stable FDG uptake. The FDG-PET scan was conducted for 30 min on high-resolution research tomography (HRRT [ECAT HRRT, Siemens, Knoxville, USA]; resolution, 2.5 mm full width at half maximum resolution in three-dimensional acquisition mode) under general anaesthesia maintained by a one-time injection of tiletamine/zolazepam (8 mg/kg *i.v.* Zoletil, Virbac, Carros, France) following medetomidine (20 µg/kg *i.m.*; Domitor, Pfizer, Seoul, Republic of Korea) premedication. After PET scanning, the dog was injected again with tiletamine/zolazepam (8 mg/kg *i.v.*) for the MR scan. Therefore, the total duration of anaesthesia was 1 h for the PET-MRI scan. A shuttle system was used to transport the dog to a 7 T-MRI scanner (Magnetom 7T, Siemens, Berlin, Germany), and then pre-contrast and post-contrast T1-weighted three-dimensional magnetisation-prepared rapid gradient echo images

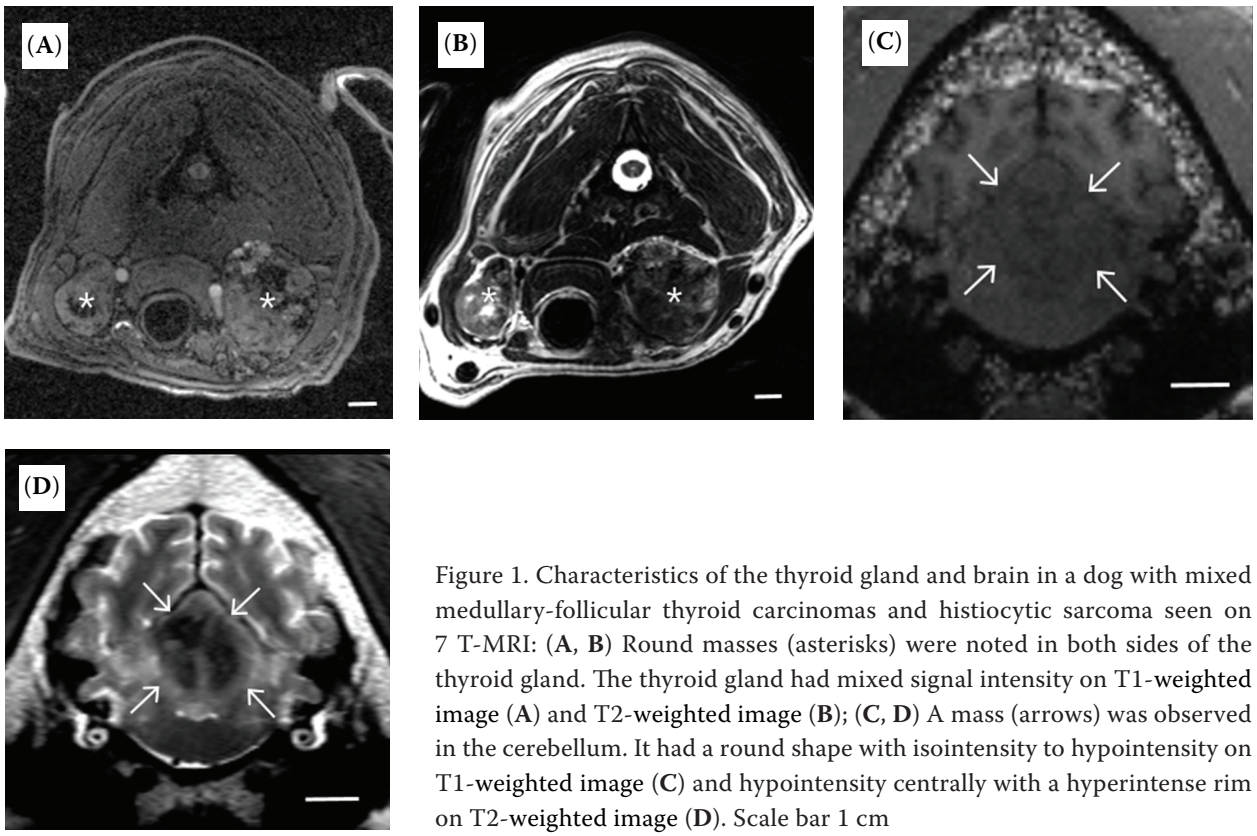

Figure 1. Characteristics of the thyroid gland and brain in a dog with mixed medullary-follicular thyroid carcinomas and histiocytic sarcoma seen on 7 T-MRI: (**A**, **B**) Round masses (asterisks) were noted in both sides of the thyroid gland. The thyroid gland had mixed signal intensity on T1-weighted image (**A**) and T2-weighted image (**B**); (**C**, **D**) A mass (arrows) was observed in the cerebellum. It had a round shape with isointensity to hypointensity on T1-weighted image (**C**) and hypointensity centrally with a hyperintense rim on T2-weighted image (**D**). Scale bar 1 cm

doi: 10.17221/8/2017-VETMED

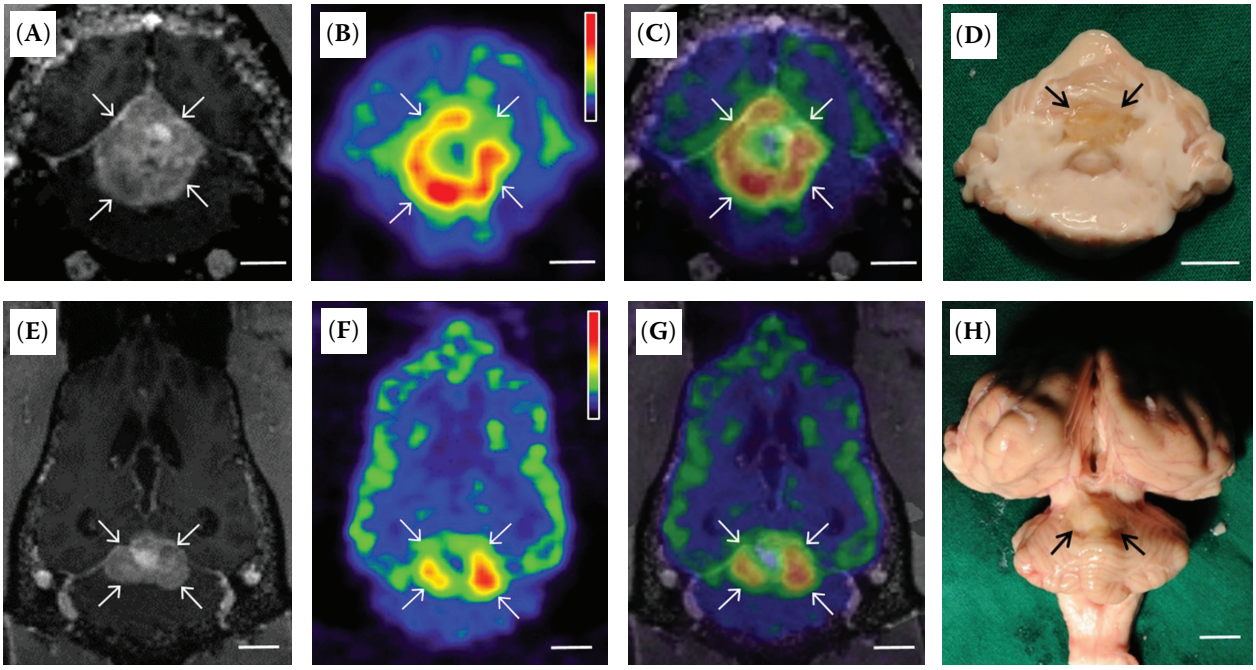

Figure 2. Characteristics of intracranial histiocytic sarcoma seen on 7 T-MRI/^{18}F-fluorodeoxyglucose-positron emission tomography and necropsy findings. Transverse (**A**–**D**) and dorsal (**E**–**H**) images of the brain are pictured. (**A**, **E**) On post-contrast T1-weighted image, an enhanced mass (arrows) was observed in the cerebellar vermis. (**B**, **F**) ^{18}F-fluorodeoxyglucose-positron emission tomography images demonstrated an area of high ^{18}F-fluorodeoxyglucose uptake with a reddish-to-yellowish colour (arrows) in the cerebellum. The colour bar expresses standardised uptake value [minimum (black): 0, maximum (red): 10]. (**C**, **G**) The anatomical location of the hypermetabolic area (arrows) was clearly identified by combining 7 T-MRI images with positron emission tomography images. (**D**, **H**) At necropsy, a nodular mass (arrows) was found in the cerebellar vermis. Scale bar 1 cm

(TR 4000 ms, TE 2.95 ms, TI 1100 ms, flip angle 10°, matrix 256 × 256, FOV 192 mm × 192 mm, slice thickness 0.75 mm) and transverse T2-weighted turbo spin echo images (TR 15,000 ms, TE 69 ms, flip angle 90°, matrix 512 × 464, FOV 220 mm × 200 mm, slice thickness 2.5 mm, interslice gap 2.5 mm) of the brain and neck were obtained. Because the strong magnetic field of 7 T-MRI and the electronics of PET could influence image quality, PET and MRI were performed separately under the optimal operating conditions for each system.

The 7 T-MRI scan of the thyroid gland lesions demonstrated mixed signal intensity on T1 and T2-WI (Figures 1A and 1B). As in the first MRI scan, the cerebellar mass was spherical and well defined, with hypointensity on T1-WI (Figure 1C) and hypointensity centrally with a poorly defined, hyperintense rim around the mass on T2-WI (Figure 1D). These thyroid and cerebellar masses were enhanced on post-contrast T1-WI (Figures 2A, 2E, 3A and 3E). The diameter (19 mm) of the mass and enhanced area was increased in comparison with the first scan (15–17 mm).

The FDG uptake of the cerebellar and thyroid lesions was elevated on the HRRT-PET scan (Figures 2B, 2F, 3B, and 3F). The standardised uptake value (SUV) was higher in the cerebellum (SUV: 6.16) and thyroid gland (SUV: 3.72) than in the occipital cortex (SUV: 3.92) and mandibular salivary gland (SUV: 1.34), respectively. The anatomical location of the hypermetabolic lesions could be more precisely identified in the PET-MRI fusion images (Figures 2C, 2G, 3C and 3G).

Clinical signs slowly improved with an additional three cycles of chemotherapy. At 109 days after the first treatment, new subcutaneous nodules were identified on the sternum, axilla and abdomen. Fine-needle aspiration of these skin lesions revealed malignant round cells with prominent nuclei, increased pleomorphism and bizarre mitotic figures. Additionally, abdominal ultrasonography demonstrated mixed echogenic nodules and a hypoechoic nodule in the liver and spleen, respectively. Three

doi: 10.17221/8/2017-VETMED

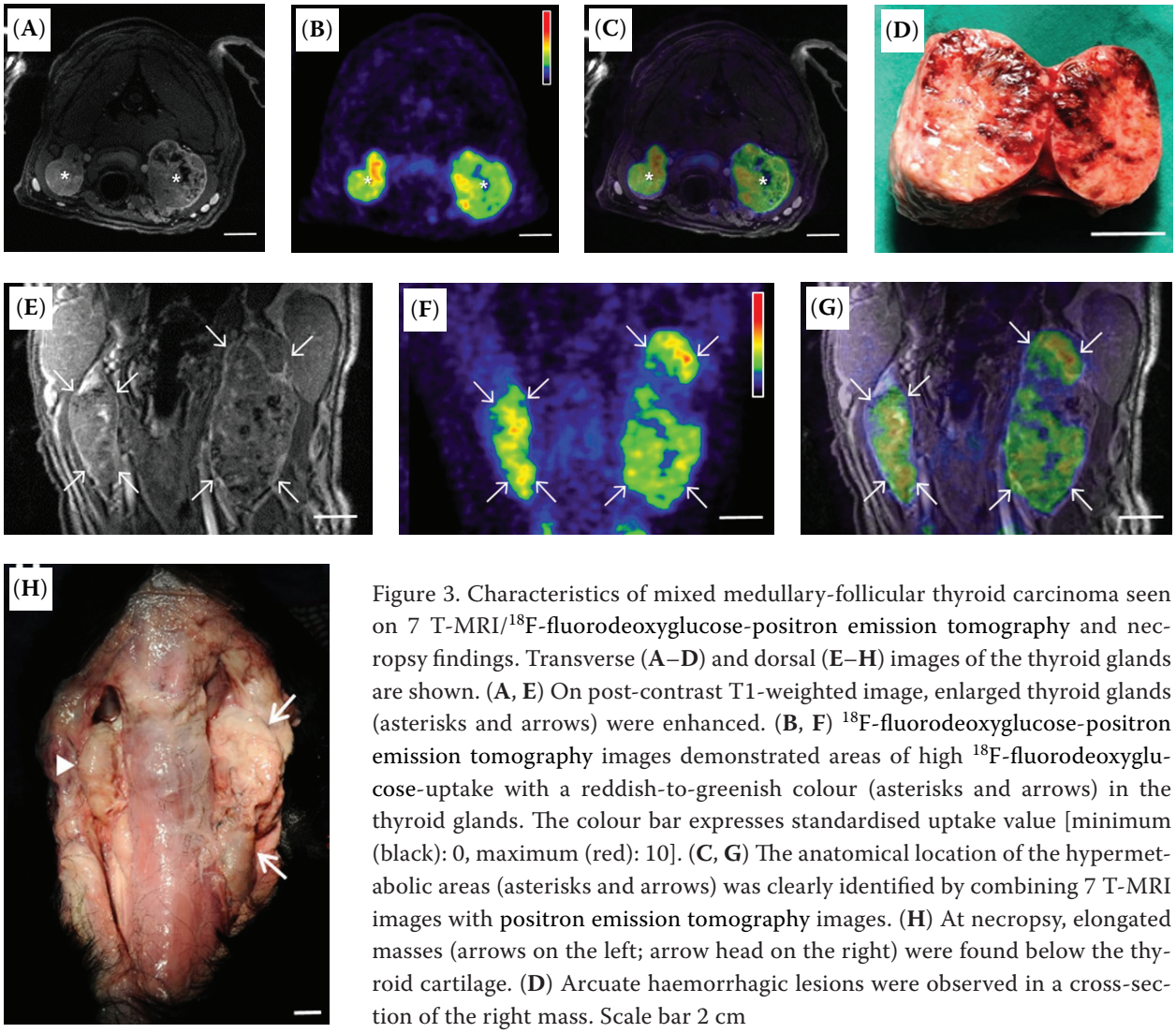

Figure 3. Characteristics of mixed medullary-follicular thyroid carcinoma seen on 7 T-MRI/^{18}F-fluorodeoxyglucose-positron emission tomography and necropsy findings. Transverse (**A**–**D**) and dorsal (**E**–**H**) images of the thyroid glands are shown. (**A**, **E**) On post-contrast T1-weighted image, enlarged thyroid glands (asterisks and arrows) were enhanced. (**B**, **F**) ^{18}F-fluorodeoxyglucose-positron emission tomography images demonstrated areas of high ^{18}F-fluorodeoxyglucose-uptake with a reddish-to-greenish colour (asterisks and arrows) in the thyroid glands. The colour bar expresses standardised uptake value [minimum (black): 0, maximum (red): 10]. (**C**, **G**) The anatomical location of the hypermetabolic areas (asterisks and arrows) was clearly identified by combining 7 T-MRI images with positron emission tomography images. (**H**) At necropsy, elongated masses (arrows on the left; arrow head on the right) were found below the thyroid cartilage. (**D**) Arcuate haemorrhagic lesions were observed in a cross-section of the right mass. Scale bar 2 cm

days after the appearance of the cutaneous nodules, the dog succumbed to hepatotoxicity, anaemia and coagulopathy.

On post-mortem examination, a cerebellar mass (diameter: 11 mm; Figures 2D and 2H) and enlargement of the thyroid glands (length × diameter: 82 mm × 38 mm on the left, 68 mm × 27 mm on the right; Figures 3D and 3H) and regional lymph nodes (submandibular and medial retropharyngeal) were confirmed. Metastatic nodular lesions of the lung, liver and spleen were accompanied by hepatosplenomegaly that was not observed in the initial evaluation using various imaging modalities. Tissue specimens of the cerebellum, thyroid, lung, liver, spleen, skin and regional lymph nodes were fixed in 10% neutral-buffered formalin, embedded in paraffin, sectioned at 4 µm and stained with haematoxylin and eosin. Microscopically, large, markedly pleomorphic discrete cells, each containing a round-to-oval nucleus, were observed in the cerebellum, liver, spleen and skin (Figures 4A–4D). Sections of the thyroid gland, lung and lymph nodes stained with haematoxylin and eosin demonstrated a follicular-compact cellular type of carcinoma (Figures 4E and 4F). Immunostaining with a histiocytic marker (CD18) was positive for pleomorphic cells in the cerebellum, liver, spleen and skin (Figures 5A–5D), whereas the thyroid and lung carcinoma stained positive for E-cadherin, thyroglobulin (Figures 5E and 5F) and calcitonin (Figures 5G and 5H). The cerebellum, liver, spleen and skin sections were negative for CD3, CD79a, E-cadherin, thyroglobulin and calcitonin. Additionally, tumour cells of the thyroid and lung were negative for CD18. Therefore, concurrent development of disseminated HS and MMFC was

doi: 10.17221/8/2017-VETMED

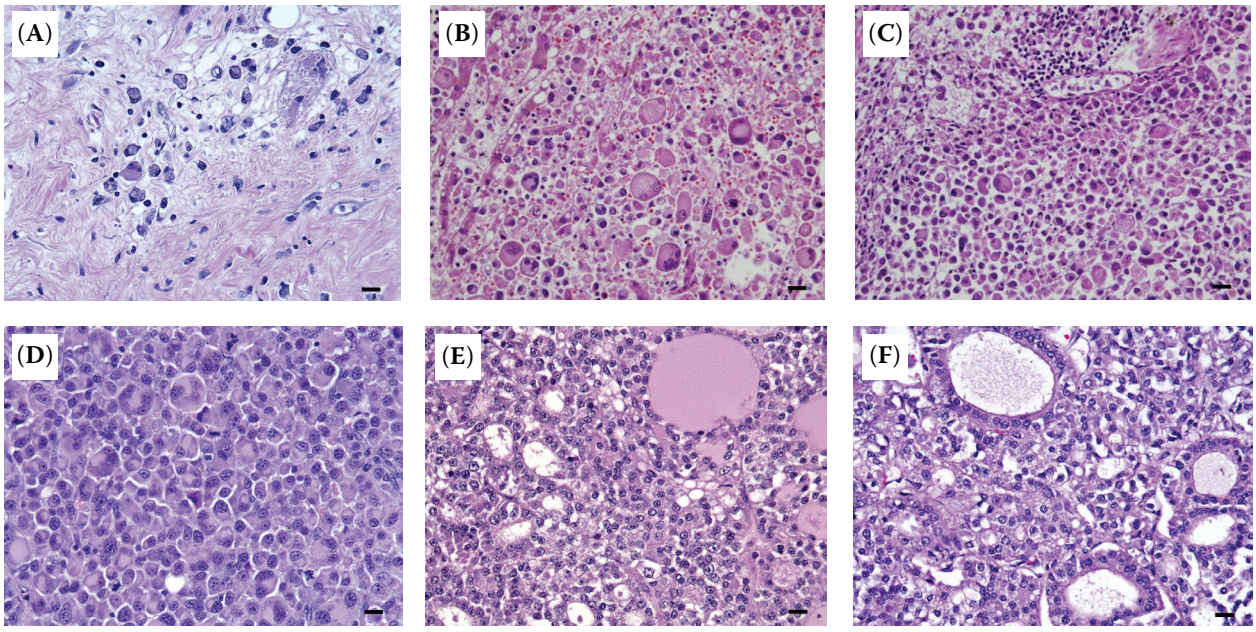

Figure 4. Photomicrographs of concurrent disseminated histiocytic sarcoma and mixed medullary-follicular thyroid carcinoma in a dog. Large, markedly pleomorphic, discrete cells containing a round-to-oval nucleus are observed in the cerebellum (**A**), liver (**B**), spleen (**C**) and skin (**D**). (**E**) The thyroid gland mass consisted of tumour cells with mixed solid-follicular pattern. (**F**) Lung nodules were composed of similar tumour cells identified in the thyroid gland. Haematoxylin and eosin stain; × 400, scale bar 15 μm

confirmed on the basis of clinical progression and imaging and histopathology findings.

DISCUSSION AND CONCLUSIONS

In the present case, the disseminated HS could be primarily localised to the cerebellum using various imaging modalities, namely, ultrasonography, CT, MRI and FDG-PET. The necropsy and histopathology revealed extraneural metastasis of a cerebellar HS to the liver, spleen and skin. Intracranial neoplasia is frequently encountered in dogs, but localised HS rarely develops in the brain (Chandra and Ginn 1999; Snyder et al. 2006; Kang et al. 2009; Tamura 2009). The prevalence of HS confined to the brain was reported to be 0.05% among dogs examined post-mortem, representing 2.2% of primary intracranial neoplasms (Song et al. 2013). In the present case, the cerebellum was the only organ affected by HS on initial examination.

In disseminated HS, secondary involvement of the central nervous system has been observed in dogs, but the brain is not considered to be one of the primary sites (Thio et al. 2006; Snyder et al. 2008). However, in this case, localised HS was first found in the cerebellum, then multiple lesions of disseminated HS were observed in the liver, spleen and skin. The dog initially presented with neurological signs, whereas other symptoms indicating systemic involvement, such as anorexia, lethargy and dyspnoea, were not noted at that time. Additionally, initial clinical staging with blood analysis and abdominal imaging did not reveal signs of metastasis, such as cytopaenia or hepatosplenomegaly. The neck masses and pulmonary nodules were confirmed to be thyroid carcinoma unrelated to the intracranial HS. Because of the highly aggressive behaviour of the malignancy, extensive disease involving multiple organs is frequently found on evaluation or necropsy of most dogs with disseminated HS. Thus, it is difficult to differentiate a primary multicentric origin from widespread metastasis of a single histiocytic malignancy (Affolter and Moore 2002). Despite this difficulty, the primary site in this case was found to be the cerebellum based on a localised cerebellar HS on the initial evaluation, late appearance of multiorgan abnormalities, findings at necropsy and results of histopathology.

To the authors' knowledge, metastasis from brain tumours has not yet been reported in dogs. A previ-

doi: 10.17221/8/2017-VETMED

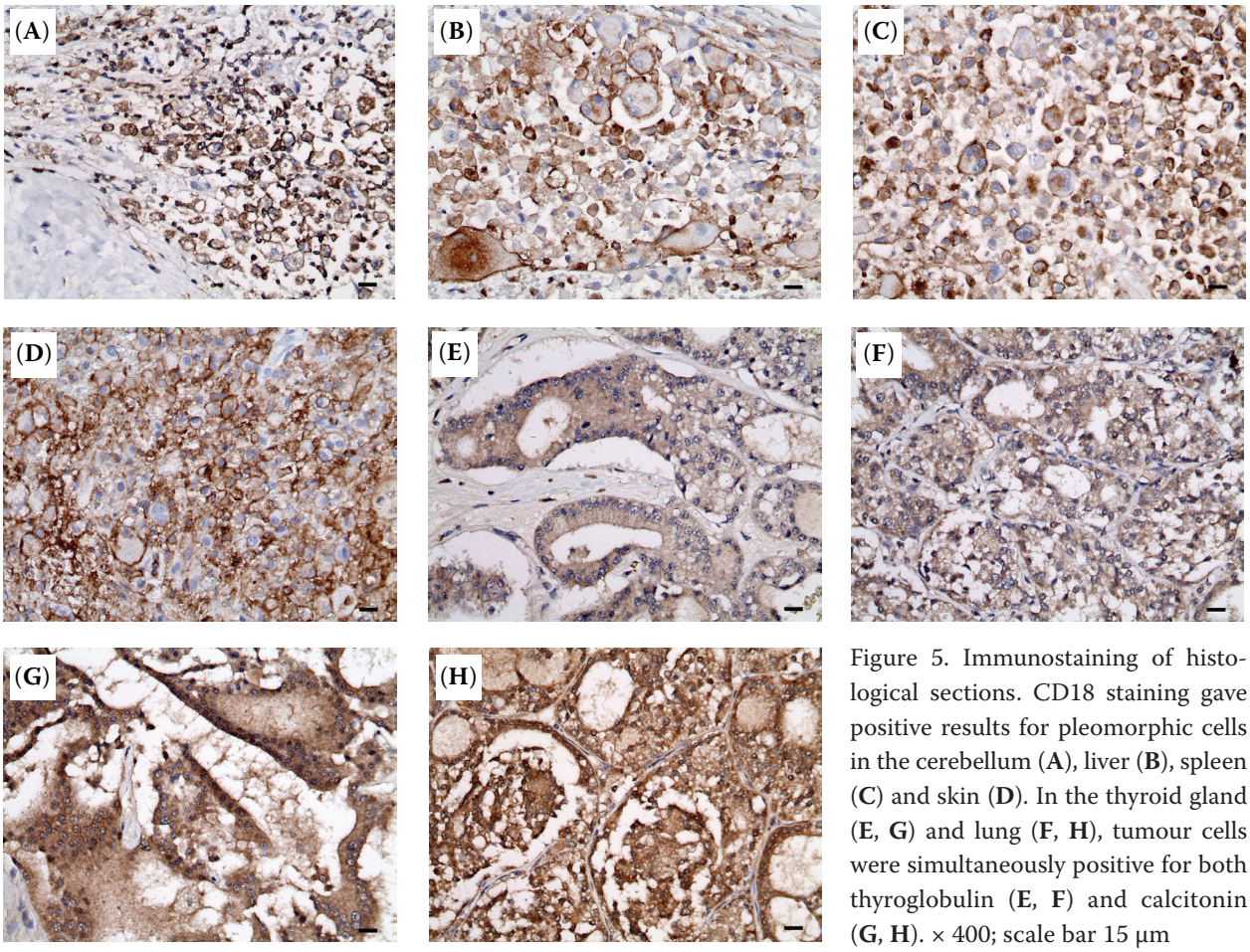

Figure 5. Immunostaining of histological sections. CD18 staining gave positive results for pleomorphic cells in the cerebellum (**A**), liver (**B**), spleen (**C**) and skin (**D**). In the thyroid gland (**E**, **G**) and lung (**F**, **H**), tumour cells were simultaneously positive for both thyroglobulin (**E**, **F**) and calcitonin (**G**, **H**). × 400; scale bar 15 μm

ous study of a primary intracranial tumour demonstrated no evidence of extracranial metastasis in dogs (Snyder et al. 2006). In humans, the incidence of somatic malignancies metastasising to the brain is approximately 10%, whereas extraneural metastasis of brain tumours is less common, occurring in up to 4.3% of cases (Houston et al. 2000; Subramanian et al. 2002). This rare occurrence of metastasis to an extracranial site is explained by the local environment and inherent characteristics of the brain tumour cells, such as invasion-related gene mutations, absence of lymphatic channels, a resistant outer dura mater, interendothelial tight junctions of the blood-brain barrier, the immune response mounted against tumour cells and a survival time which is too short to allow development of extraneural metastases (Schweitzer et al. 2001; Subramanian et al. 2002). Nevertheless, spread of tumour cells outside the brain can occur through haematological, lymphatic, and cerebrospinal pathways (Schweitzer et al. 2001). Because the blood-brain barrier in the vicinity of brain tumours is not intact, the migration of neoplastic cells into blood vessels is possible via a defective endothelial basement membrane (Kung et al. 1969; Nir et al. 1989). In primary intracranial HS affecting dogs, the most common feature on MRI is contrast enhancement, indicating increased permeability of the blood-brain barrier (Tamura et al. 2009; Mariani et al. 2015). In accordance with this feature seen on MRI, the cerebellar HS was enhanced after administration of contrast, so a haematogenous route is suspected to be one of the metastatic pathways involved in the present case. Further investigation is required to identify the mechanisms underlying intravasation of tumour cells, metastasis and peripheral tumour growth in dogs with intracranial HS.

Immunophenotyping has been used to help in determining the cell origin of HS (Fulmer and Mauldin 2007; Coomer and Liptak 2008). Generally, immunophenotypes of HS are expected to be positive for CD18 (histiocytes) and negative for CD3 (T cells), CD79a (B cells), E-cadherin (Langerhans cells) and CD45RA (B cells and naive T cells) in formalin-fixed

doi: 10.17221/8/2017-VETMED

tissue (Fulmer and Mauldin 2007). In the present case, histiocytic origin could be confirmed by positive expression of CD18 and lack of expression of CD3, CD79a and E-cadherin in the cerebellum, liver, spleen and skin. Although immunophenotypes of intracranial HS have been reported using various markers, cellular origin and histogenesis remain uncertain because of the rarity of this type of tumour (Thongtharb et al. 2016; Zanelli et al. 2017).

Follicular thyroid carcinomas are classified as follicular, compact, follicular-compact, papillary, poorly differentiated, undifferentiated and carcinosarcoma according to the World Health Organization classification of thyroid tumours in dogs (Kiupel et al. 2008). Microscopically, medullary thyroid carcinoma could be misdiagnosed as follicular carcinoma of the compact type. Therefore, immunostaining for calcitonin or markers of parafollicular cells is important for identification of medullary carcinoma, whereas thyroglobulin immunoreactivity is specific for follicular carcinoma (Campos et al. 2014). Based on microscopic observation alone the present case was initially diagnosed as a follicular-compact cellular type of carcinoma; however, the dog was definitively diagnosed as having MMFC based on dual staining for both thyroglobulin and calcitonin.

MMFC accounts for less than 0.5% of thyroid tumours in humans (Papotti et al. 1997). Although medullary thyroid carcinoma accounts for 16–36% of thyroid carcinomas in dogs, the incidence of canine MMFC is unknown (Leblanc et al. 1991; Carver et al. 1995; Campos et al. 2014). Only seven sporadic cases have been reported in dogs (Moore et al. 1984; Brown et al. 2001; Campos et al. 2014). Metastasis is common in thyroid carcinomas, and the most common metastatic sites are the lungs and regional lymph nodes (Liptak 2007; Campos et al. 2014). In this case, thyroid tumour cells were observed in the lungs and in the submandibular and medial retropharyngeal lymph nodes. A previous study demonstrated no difference in rates of metastasis between follicular and medullary carcinomas in dogs at diagnosis (Campos et al. 2014). Further study is needed to investigate the prognostic relevance of differentiating MMFC from other types of thyroid tumours with immunostaining.

The incidence of other unrelated neoplasia was estimated to be 23% in dogs with primary intracranial tumours (Snyder et al. 2006). In dogs with intracranial HS, detection of concurrent adrenal adenoma, haemangiosarcoma, melanoma, testicular seminoma and trichoepithelioma has been reported (Snyder et al. 2008; Mariani et al. 2015). Although one report described a concurrent case of thyroid carcinoma and disseminated HS, tumour cells originating from HS did not invade the brain, and classification of the thyroid carcinoma was not done by immunostaining (Scruggs et al. 2015).

FDG-PET is a molecular imaging modality for tumour staging, detection of recurrence and monitoring response to treatment. The fusion of PET with CT (PET/CT) is widely used to complement the low spatial resolution of PET images (Lawrence et al. 2010). However, CT has a number of shortcomings in soft tissue imaging; therefore, MRI can be utilised for precise anatomical localisation of malignant lesions as an alternative to CT (Cho et al. 2008). Clinical application of PET/CT has been reported in a number of dogs with spontaneously occurring tumours (Seiler et al. 2015), whereas use of PET/MRI in canines is limited to the healthy or epileptic brain, intracranial HS and pituitary microtumours (Kang et al. 2009; Kang et al. 2012; Jokinen et al. 2014; Son et al. 2015). In the present case, 7 T-MRI clearly visualised the cerebellar and thyroid lesions, thus helping in the identification of the anatomical location of the hypermetabolic lesions on PET. A consensus on the interpretation of FDG uptake by the brain and thyroid gland has yet to be reached, so further investigation of PET/MRI is necessary in dogs with spontaneously occurring brain and thyroid tumours.

In conclusion, the present case was diagnosed as concurrent MMFC and disseminated HS based on clinical progression and imaging and histopathology findings. Therefore, the brain could be considered as one of the primary sites for disseminated HS. In addition to follicular and medullary type carcinoma, classification of MMFC may require immunostaining for markers of follicular and parafollicular cells. While high-resolution PET/MRI could be applied for identification of brain and thyroid tumours in dogs, it was not used for tumour staging due to the limitation of the whole-body scan.

REFERENCES

Affolter VK, Moore PF (2002): Localized and disseminated histiocytic sarcoma of dendritic cell origin in dogs. Veterinary Pathology 39, 74–83.

doi: 10.17221/8/2017-VETMED

Brown PJ, Rema A, Gartner F (2001): Thyroglobulin, calcitonin, Ki 67 and CEA immunohistochemical staining of dog thyroid carcinomas. European Journal of Veterinary Pathology 7, 11–16.

Campos M, Ducatelle R, Rutteman G, Kooistra HS, Duchateau L, de Rooster H, Peremans K, Daminet S (2014): Clinical, pathologic, and immunohistochemical prognostic factors in dogs with thyroid carcinoma. Journal of Veterinary Internal Medicine 28, 1805–1813.

Carver JR, Kapatkin A, Patnaik AK (1995): A comparison of medullary thyroid carcinoma and thyroid adenocarcinoma in dogs: a retrospective study of 38 cases. Veterinary Surgery 24, 315–319.

Chandra AM, Ginn PE (1999): Primary malignant histiocytosis of the brain in a dog. Journal of Comparative Pathology 121, 77–82.

Cho ZH, Son YD, Kim HK, Kim KN, Oh SH, Han JY, Hong IK, Kim YB (2008): A fusion PET-MRI system with a high-resolution research tomograph-PET and ultra-high field 7.0 T-MRI for the molecular-genetic imaging of the brain. Proteomics 8, 1302–1323.

Coomer AR, Liptak JM (2008): Canine histiocytic diseases. Compendium: Continuing Education for Veterinarians 30, 202–204, 208–216.

Fulmer AK, Mauldin GE (2007): Canine histiocytic neoplasia: an overview. Canadian Veterinary Journal 48, 1041–1043.

Hales M, Rosenau W, Okerlund MD, Galante M (1982): Carcinoma of the thyroid with a mixed medullary and follicular pattern: morphologic, immunohistochemical, and clinical laboratory studies. Cancer 50, 1352–1359.

Houston SC, Crocker IR, Brat DJ, Olson JJ (2000): Extraneural metastatic glioblastoma after interstitial brachytherapy. International Journal of Radiation Oncology Biology Physics 48, 831–836.

Jokinen TS, Haaparanta-Solin M, Viitmaa R, Gronroos TJ, Johansson J, Bergamasco L, Snellman M, Metsahonkala L (2014): FDG-PET in healthy and epileptic Lagotto Romagnolo dogs and changes in brain glucose uptake with age. Veterinary Radiology and Ultrasound 55, 331–341.

Kang BT, Park C, Yoo JH, Gu SH, Jang DP, Kim YB, Woo EJ, Kim DY, Cho ZH, Park HM (2009): 18F-fluorodeoxyglucose positron emission tomography and magnetic resonance imaging findings of primary intracranial histiocytic sarcoma in a dog. Journal of Veterinary Medical Science 71, 1397–1401.

Kang BT, Son YD, Lee SR, Jung DI, Kim DE, Chang KT, Cho ZH, Park HM (2012): FDG uptake of normal canine brain assessed by high-resolution research tomography-positron emission tomography and 7 T-magnetic resonance imaging. Journal of Veterinary Medical Science 74, 1261–1267.

Kiupel M, Capen C, Miller M, Smedley R (2008): Histological classification of the endocrine system of domestic animals. In: Schulman FY (ed.): WHO International Histological Classification of Tumors of Domestic Animals. Armed Forces Institute of Pathology. 25–39.

Kung PC, Lee JC, Bakay L (1969): Vascular invasion by glioma cells in man: an electron microscopic study. Journal of Neurosurgery 31, 339–345.

Lawrence J, Rohren E, Provenzale J (2010): PET/CT today and tomorrow in veterinary cancer diagnosis and monitoring: fundamentals, early results and future perspectives. Veterinary and Comparative Oncology 8, 163–187.

Leblanc B, Parodi AL, Lagadic M, Hurtrel M, Jobit C (1991): Immunocytochemistry of canine thyroid tumors. Veterinary Pathology 28, 370–380.

Liptak JM (2007): Canine thyroid carcinoma. Clinical Techniques in Small Animal Practice 22, 75–81.

Mariani CL, Jennings MK, Olby NJ, Borst LB, Brown Jr JC, Robertson ID, Seiler GS, MacKillop E (2015): Histiocytic sarcoma with central nervous system involvement in dogs: 19 cases (2006–2012). Journal of Veterinary Internal Medicine 29, 607–613.

Moore PF (2014): A review of histiocytic diseases of dogs and cats. Veterinary Pathology 51, 167–184.

Moore FM, Kledzik GS, Wolfe HJ, DeLellis RA (1984): Thyroglobulin and calcitonin immunoreactivity in canine thyroid carcinomas. Veterinary Pathology 21, 168–173.

Nir I, Levanon D, Iosilevsky G (1989): Permeability of blood vessels in experimental gliomas: uptake of 99mTc-glucoheptonate and alteration in blood-brain barrier as determined by cytochemistry and electron microscopy. Neurosurgery 25, 523–531.

Papotti M, Negro F, Carney JA, Bussolati G, Lloyd RV (1997): Mixed medullary-follicular carcinoma of the thyroid. A morphological, immunohistochemical and in situ hybridization analysis of 11 cases. Virchows Archiv 430, 397–405.

Pfaltz M, Hedinger CE, Muhlethaler JP (1983): Mixed medullary and follicular carcinoma of the thyroid. Virchows Archiv 400, 53–59.

Sadow PM, Hunt JL (2010): Mixed medullary-follicular-derived carcinomas of the thyroid gland. Advances in Anatomic Pathology 17, 282–285.

Schweitzer T, Vince GH, Herbold C, Roosen K, Tonn JC (2001): Extraneural metastases of primary brain tumors. Journal of Neuro-Oncology 53, 107–114.

Scruggs JL, Nobrega-Lee M, Fry MM, Applegate R (2015): Hypercalcemia and parathyroid hormone-related peptide expression in a dog with thyroid carcinoma and histiocytic sarcoma. Veterinary Clinical Pathology 44, 249–252.

doi: 10.17221/8/2017-VETMED

Seiler SM, Baumgartner C, Hirschberger J, Beer AJ, Bruhschwein A, Kreutzmann N, Laberke S, Wergin MC, Meyer-Lindenberg A, Brandl J, von Thaden AK, Farrell E, Schwaiger M (2015): Comparative oncology: evaluation of 2-deoxy-2-[18F]fluoro-D-glucose (FDG) positron emission tomography/computed tomography (PET/CT) for the staging of dogs with malignant tumors. PLoS One 10, doi: 10.1371/journal.pone.0127800.

Snyder JM, Shofer FS, Van Winkle TJ, Massicotte C (2006): Canine intracranial primary neoplasia: 173 cases (1986–2003). Journal of Veterinary Internal Medicine 20, 669–675.

Snyder JM, Lipitz L, Skorupski KA, Shofer FS, Van Winkle TJ (2008): Secondary intracranial neoplasia in the dog: 177 cases (1986–2003). Journal of Veterinary Internal Medicine 22, 172–177.

Son YD, Kim DJ, Kang JH, Chang DW, Jin YB, Jung DI, Lee C, Yang MP, Lee SR, Kang BT (2015): High-resolution fluorodeoxyglucose positron emission tomography and magnetic resonance imaging findings of a pituitary microtumor in a dog. Irish Veterinary Journal 68, doi: 10.1186/s13620-015-0050-5.

Song RB, Vite CH, Bradley CW, Cross JR (2013): Postmortem evaluation of 435 cases of intracranial neoplasia in dogs and relationship of neoplasm with breed, age, and body weight. Journal of Veterinary Internal Medicine 27, 1143–1152.

Subramanian A, Harris A, Piggott K, Shieff C, Bradford R (2002): Metastasis to and from the central nervous system – the 'relatively protected site'. Lancet Oncology 3, 498–507.

Tamura S, Tamura Y, Nakamoto Y, Ozawa T, Uchida K (2009): MR imaging of histiocytic sarcoma of the canine brain. Veterinary Radiology and Ultrasound 50, 178–181.

Thio T, Hilbe M, Grest P, Pospischil A (2006): Malignant histiocytosis of the brain in three dogs. Journal of Comparative Pathology 134, 241–244.

Thongtharb A, Uchida K, Chambers JK, Kagawa Y, Nakayama H (2016): Histological and immunohistochemical studies on primary intracranial canine histiocytic sarcomas. Journal of Veterinary Medical Science 78, 593–599.

Wucherer KL, Wilke V (2010): Thyroid cancer in dogs: an update based on 638 cases (1995–2005). Journal of the American Animal Hospital Association 46, 249–254.

Zanelli M, Ragazzi M, Marchetti G, Bisagni A, Principi M, Fanni D, Froio E, Serra S, Zanetti E, De Marco L, Giangaspero F, Ascani S (2017): Primary histiocytic sarcoma presenting as diffuse leptomeningeal disease: Case description and review of the literature. Neuropathology [Online first], doi: 10.1111/neup.12390.

Received: January 13, 2017
Accepted after corrections: September 20, 2017